doi:10.14311/ppt.2025.2.158
*Plasma Physics and Technology* **12**(2):158–163, 2025 

# OPTICAL EMISSION SPECTROSCOPY EVALUATION OF EXHAUST GAS TEMPERATURES AFTER HIGH CURRENT INTERRUPTION IN $CO_2/O_2$

J. T. Engelbrecht*, A. Frank, P. Pietrzak

*Hitachi Energy Research, 5405 Baden-Dättwil, Switzerland*

* joey.engelbrecht@hitachienergy.com

**Abstract.** In high voltage gas circuit breakers, the pressure buildup necessary for arc extinguishing is partially generated by ablated PTFE nozzle material, which mixes with the insulating gas before being blown through the arcing zone during current interruption. When high short-circuit currents are interrupted, this mixture can retain elevated temperatures for milliseconds as it expands into the circuit breaker's exhaust volume, and therefore needs to be effectively managed to ensure adequate insulation is maintained. From a circuit breaker design standpoint, this makes accurate knowledge of the exhaust temperature immediately after current zero essential. In this work, two optical emission spectroscopy based temperature determination methods were applied to study the temperature near the exhaust plane exit in a $CO_2/O_2$-filled model circuit breaker near current zero. The measured broadband spectra show strong continuum emission from soot particles, in addition to band emission from CuF molecules formed in the exhaust gas. Gray-body spectral fits were performed to estimate temperatures from the continuum emission, which is dominated by the high emissivity soot particles, while temperatures were also obtained via Boltzmann plot evaluation of the emission band intensity ratios. The two methods reveal a temperature mismatch that may suggest slower cooling of the larger soot particles in comparison to the rest of the exhaust gas mixture.

**Keywords:** high-voltage circuit breaker, $SF_6$ alternatives, optical emission spectroscopy, CuF.

## 1. Introduction

Circuit breakers (CBs) play essential roles in the electric power grid, where they must switch currents and provide insulation over a wide range of conditions that can occur in the network. At high transmission-level voltages, pressurized $SF_6$ has long been the dominant insulation and switching medium used in HVCBs, however recent research has focused on the development of more eco-friendly gas alternatives which are now available on the market [1]. Most of these products use a base gas mixture of $CO_2/O_2$, with admixtures of C4-FN possible depending on the specific application.

One critical task of HVCBs is the successful interruption of high short-circuit currents. By design, the high current arc formed during these switching events ablates a significant amount of material from the insulating nozzle and arcing contacts of the CB. This material is directed into a heating volume where it mixes with surrounding gas, raising its temperature to several thousand kelvin [2]. During interruption, this mixture is blown through the arc and exhausted into the main gas volume, resulting in a severe reduction of gas density in affected regions [3]. For metal-enclosed CBs to support the fast-rising transient overvoltages that accompany these faults, the hot exhaust gas must be cooled or redirected in order to prevent it from compromising the electrical insulation between the energized exhaust tube and the grounded enclosure [4]. Effective gas management solutions thus require accurate information about the temperature distribution of the exhaust gas, particularly during the important time window surrounding current zero (CZ).

In this work, an optical emission spectroscopy system was used to diagnose exhaust gas temperatures in a model circuit breaker. Experiments were carried out in a $CO_2/O_2$ mixture at arcing currents of up to 100 kA. Optical measurements were performed in the critical region near the exhaust tube exit during the time window immediately after CZ. Two methods are demonstrated to extract temperatures from the measured spectra, using continuum emission and line emission respectively. A complete set of results obtained using both methods is presented and critically examined herein.

## 2. Methods

### 2.1. Experimental setup

A sketch of the self-blast model circuit breaker is presented in Fig. 1, showing the interrupter region, including Cu-W arcing contacts enclosed within an insulating nozzle made from PTFE. The left side of the figure depicts the moving part: a puffer cylinder to which the tulip contact and nozzle are mechanically coupled. The opening stroke compresses the enclosed volume against a stationary piston, contributing a portion of the pressure buildup generated inside the test device. This motion also separates the contacts, drawing a switching arc under an applied current. On the right side, a stationary tube surrounds the plug contact, guiding the exhaust gas to the measurement region at the rear of the test vessel.

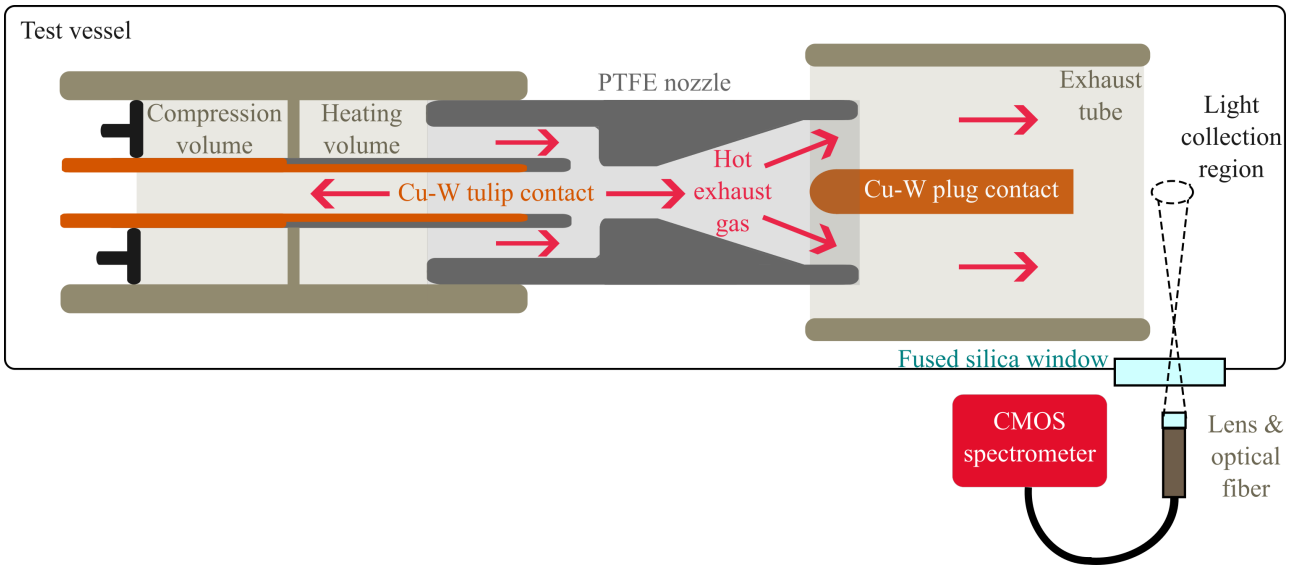


*Figure 1. Sketch of model circuit breaker setup showing cut-away view of gas flow path through heating volume, arcing region, and exhaust region near current zero, together with diagnostic line-of-sight.*

Six arcing shots were carried out during this work. A 50 Hz sinusoidal test current with a first half-wave peak of $I \approx 100$ kA was applied. All shots were conducted with long arcing times of $t_{arc} = 14$ ms to 15 ms in order to maximize the amount of ablated material. Current interruption took place after the second half-wave, when the current amplitude had typically dropped to $I \approx 55$ kA. The intense radiation produced by the high current arc causes heavy ablation of the interior wall of the PTFE nozzle, in addition to the ends of the Cu-W arcing contacts. This introduces excess warm material into the arcing region, creating an overpressure that drives backheating, which provides the remainder of the breaker's pressure buildup. Pressure was measured experimentally inside the heating volume by a transient pressure sensor.

Fig. 1 also shows the line of sight for the optical emission spectroscopy (OES) diagnostic $\sim 1$ cm from the exhaust tube exit plane. Light from this region was collected outside of the experimental vessel by a 600 µm diameter optical fiber with a collimating lens that focused incoming light from a 1 cm diameter spot. The opposite end of the fiber was coupled to a Thorlabs CCT10 CMOS spectrometer, which measures broadband spectra from 200 nm to 1000 nm with a 2 nm resolution. Due to the low repetition rate of this device, only a single spectrum was recorded for each shot, by triggering the spectrometer at the instant of CZ and leaving the shutter open for a variable integration time $\Delta t$. A relative calibration of the OES system was performed using a quartz tungsten halogen (QTH) lamp with a color temperature of 3250 K, which was placed at the measurement location inside the experimental vessel.

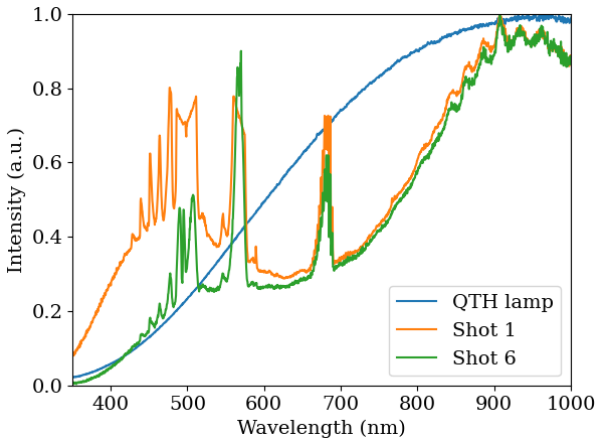


*Figure 2. Comparison of measured exhaust gas spectra with near-blackbody spectrum obtained from quartz tungsten halogen calibration lamp.*

## 2.2. Spectral temperature evaluation

### 2.2.1. Continuum emission

Fig. 2 shows the spectra from the first and last shots of the experimental series alongside a calibration lamp spectrum. Although previous studies have suggested that the spectral radiance distribution of exhaust gas under similar conditions closely resembles that of a gray-body, thanks to the presence of highly emissive soot particles [2], the measured exhaust spectra in this work clearly deviate significantly from this behavior, as they exhibit strong emission line features in addition to broader attenuation spanning much of the visible range. However, if it is assumed that the emissivity $\epsilon$ at long and short wavelengths is similar, a relative estimate of the temperature may be deduced by comparing the relative intensity of the continuum emission in the ultraviolet and infrared. In the case of Shot 6, relative intensities on both ends of

the spectrum are similar to those observed with the calibration lamp, suggesting an exhaust temperature close to the 3250 K lamp temperature, while in the case of Shot 1, the excess emission at shorter wavelengths suggests a significantly higher temperature. Temperature estimates were obtained by performing gray-body fits to Planck's radiation law,

$$B_{\mathrm{P}}(\lambda) = \frac{1}{\lambda^5} \frac{C_{\mathrm{P}}}{\exp(hc/\lambda k_{\mathrm{B}} T) - 1}, \tag{1}$$

where $C_{\mathrm{P}}$ is a fitting constant that incorporates $\epsilon$, which is assumed to be constant within the wavelength ranges used for fitting (350 nm to 435 nm and 890 nm to 1000 nm).

This approach produced reasonable fits for all measured spectra, however the deviations observed at intermediate (visible) wavelengths should also be considered to assess the accuracy of the resulting temperatures. Most troubling for the gray-body assumption is the broad, wavelength dependent attenuation observed from 500 nm to 800 nm. It is possible that this phenomenon originates from the presence of soot particles of varying size in the exhaust gas. If the particle size distribution is in a similar range to the wavelength of light, Mie scattering interactions between the two can result in a wavelength-dependent refractive index and effective emissivity $\epsilon(\lambda)$ [5, 6]. The influence of these processes on the resulting spectrum can be difficult to predict theoretically without additional knowledge of the soot composition and size distribution, which may change dynamically throughout the experiment [7]. Moreover, competing effects may arise depending on if the interaction affects the emitting particle, which can enhance emissivity, or if a scattering process occurs along the line-of-sight through the exhaust plume, resulting in attenuation.

It has been shown that standard Planck fits can result in systematic temperature overestimation when particle size effects become significant [6]. In order to bracket the uncertainty interval, a lower bound for the temperature can be estimated by considering the Rayleigh limit of very small emitting particles, which introduces a $1/\lambda$ dependence to $\epsilon$:

$$\epsilon_R(\lambda) \propto \frac{4\pi D}{\lambda}. \tag{2}$$

Assuming constant particle diameter $D$ leads to the following fit function for spectral radiance under the Rayleigh limit:

$$B_{\mathrm{R}}(\lambda) = \frac{1}{\lambda^6} \frac{C_{\mathrm{R}}}{\exp(hc/\lambda k_{\mathrm{B}} T) - 1}. \tag{3}$$

### 2.2.2. Band emission

Comparison with published spectral data revealed that all major emission features observed in the measured spectra could be attributed to electronic band transitions of CuF molecules [8–14]. Molecular data for the most prominent of the CuF transitions is compiled in Table 1. Fig. 3 shows several of these emission bands in more detail, alongside luminescence spectra of the same bands from UV photolysis experiments performed by by Talaga et al. [13]. Although the main electronic transitions noted in Table 1 can be identified and resolved, more severe spectral broadening is evident in the present results, such that in most cases it is not possible to resolve individual vibrational transitions contributing to each band. This broadening is mainly caused by the high gas fill pressures used in this experiment ($\sim 10$ bar), and is worsened by the relatively poor 2 nm instrument resolution.

| Upper state | $g_u$ | $\tau_u$ (µs) | $\lambda_0$ (nm) | $E_u$ (eV) | Ref. |
|---|---|---|---|---|---|
| $D^3\Delta_1$ | 6 | 9.25 | 439 | 2.83 | [9, 11] |
| | 6 | 9.25 | 451 | 2.76 | [9, 11] |
| | 6 | 9.25 | 463 | 2.69 | [11, 13] |
| | 6 | 9.25 | 477 | 2.60 | [11, 13] |
| $C^1\Pi$ | 2 | 0.6 | 493 | 2.52 | [8, 9] |
| $B^1\Sigma^+$ | 1 | 1.2 | 507 | 2.45 | [8, 9] |
| $A^3\Pi$ | 6 | 7.3 | 569 | 2.18 | [8, 9] |
| $a^3\Sigma^+$ | 3 | 56.2 | 681 | 1.82 | [11, 13] |

*Table 1. Electronic transition data for observed CuF emission bands. All observed bands correspond to transitions into the electronic ground state $X^1\Sigma^+$.*

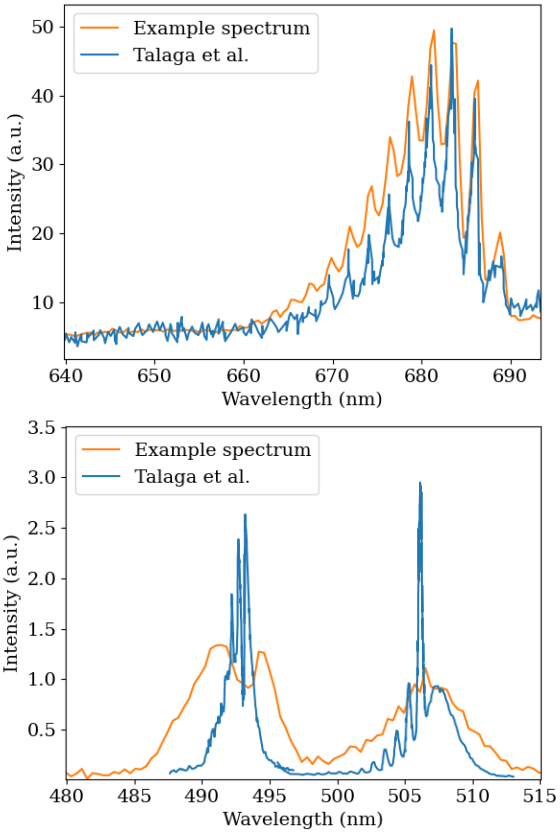


*Figure 3. Examples of CuF emission bands measured in this work, plotted together with the same bands observed by Talaga et al. At top: $a^3\Sigma^+ \rightarrow X^1\Sigma^+$, at bottom: $C^1\Pi \rightarrow X^1\Sigma^+$ and $B^1\Sigma^+ \rightarrow X^1\Sigma^+$.*

Methling et al. showed that CuF molecules can form under similar experimental conditions in a model CB through the interaction of ablated PTFE nozzle material (chemical formula $(C_2F_4)_n$) and Cu vapor from the arcing contacts, which can mix inside the heating volume [14]. In that study, the CuF features were observed only in absorption, however here strong CuF emission was observed, a distinction that may result from the much higher currents used in the present experiment (100 kA vs. 11 kA). In some cases self-reversal of the $C^1\Pi \rightarrow X^1\Sigma^+$ band was observed, as seen in Fig. 3, suggesting that sufficient unexcited CuF molecules were present along the line-of-sight for this band to appear in absorption as well.

The presence of multiple CuF emission bands in the spectra allows for determination of the exhaust gas temperature via the Boltzmann plot method [15]. This approach assumes that the excitation of CuF molecules follows a Boltzmann distribution, corresponding to specific population ratios of the excited energy levels at a given temperature. Relative level populations can be ascertained directly from the measured line intensity ratios with the appropriate molecular data, using:

$$\ln\left(\frac{I\lambda_0}{A_{ul}g_u}\right) = \frac{1}{k_B T}E_u + b_0, \tag{4}$$

where $I$ represents the spectrally integrated line intensities, $\lambda_0$ is the center wavelength, $A_{ul}$ is the transition probability, and $g_u$ is the upper state degeneracy. Plotting the LHS of Eq. 4 against $E_u$ and taking the slope thus constitutes a direct measurement of the electronic excitation temperature of the CuF molecules.

All observed CuF emission bands were found to correspond to transitions into the electronic ground state $X^1\Sigma^+$. This is consistent with the findings of other studies: transitions between excited states of CuF have not been observed experimentally [9, 13], and the theoretical calculations of Schamps et al. suggest that such transitions have a probability more than two orders of magnitude lower than corresponding ground state transitions [12]. Under these conditions, it is possible to approximate the transition probabilities $A_{ul}$ by inverting the excited state lifetimes reported in Table 1,

$$A_{ul} \approx 1/\tau_u. \tag{5}$$

The same approach was adopted by Steele et al. to determine CuF temperatures in [8].

The measured intensities represent an integration over all transitions with the same vibrational quantum number shift $\Delta\nu$. Generally for this evaluation, $\Delta\nu = 0$, with the exception of $D^3\Delta_1 \rightarrow X^1\Sigma^+$, where several bands of higher order in $\Delta\nu$ were observed. It should also be noted that the values of $\tau_u$ reported in Table 1 neglect any influence that the occupancy of different vibrational and rotational states may have on relative transition probabilities. This approximation is justified, as it was shown in [12] that the calculated electronic state lifetimes used in this work are independent of $\nu$ and show little sensitivity to the rotational level $J$.

| Shot | $p_{max}$ (a.u.) | $T_P$ (K) | $T_R$ (K) | $T_B$ (K) | $\Delta t$ (ms) |
|---|---|---|---|---|---|
| 1 | 1 | 3900 | 3300 | 2600 | 1 |
| 2 | 0.92 | 3900 | 3300 | 2600 | 0.18 |
| 3 | 0.83 | 2700 | 2300 | 2300 | 0.06 |
| 4 | 0.87 | 3100 | 2600 | 2400 | 0.06 |
| 5 | 0.83 | 3100 | 2600 | 2000 | 0.1 |
| 6 | 0.68 | 3100 | 2700 | 2100 | 1 |

*Table 2. Results from six shots performed in $CO_2/O_2$. $p_{max}$: maximum pressure measured inside the heating volume, normalized to Shot 1. $T_P$ & $T_R$: temperatures determined from fits to Eqs. (1) and (3), respectively. $T_B$: Boltzmann plot temperatures. $\Delta t$: spectral integration times for each shot, starting from CZ.*

## 3. Results

### 3.1. Exhaust temperatures

Figure 4 presents results obtained with both methods for the first and last shots of the experimental series. In some cases it was necessary to omit certain bands in Table 2 from the Boltzmann plot evaluation, due to saturation (evident for the most intense lines in Shot 1), absorption (mainly of the $C^1\Pi \rightarrow X^1\Sigma^+$ transition as seen in Fig. 3), and/or insufficient integrated intensity (affecting higher orders of $D^3\Delta_1 \rightarrow X^1\Sigma^+$ in some cases). At least five measured bands were used to produce each Boltzmann plot, with all plots exhibiting reliable linearity.

Table 2 summarizes the results from all six shots. The first two shots, which produced the largest pressure buildup in the heating volume, generated the highest temperatures according to both evaluation methods. Ablation of the PTFE nozzle led to lower pressures for later shots, generally resulting in lower measured exhaust temperatures, with values of $T_P$ falling from approximately 4000 K to 3000 K. The CuF excitation temperatures ($T_B$) were substantially lower than $T_P$, with values dropping from 2600 K to 2000 K over the shot series. Temperatures from the Rayleigh fits ($T_R$) are only $\sim$ 15% lower than $T_P$, meaning that the choice of spectral emission function alone does not explain the large temperature discrepancy with the Boltzmann plots.

### 3.2. Uncertainty assessment

In order to discuss the significance of the temperature mismatch, the experimental uncertainties must be estimated. In the continuum emission evaluation, an effort was made to bracket the uncertainty interval by providing values for $T_P$ and $T_R$, representing upper and lower limits, respectively, resulting in $\sim \pm 10\%$ uncertainty. While this provides an adequate estimate

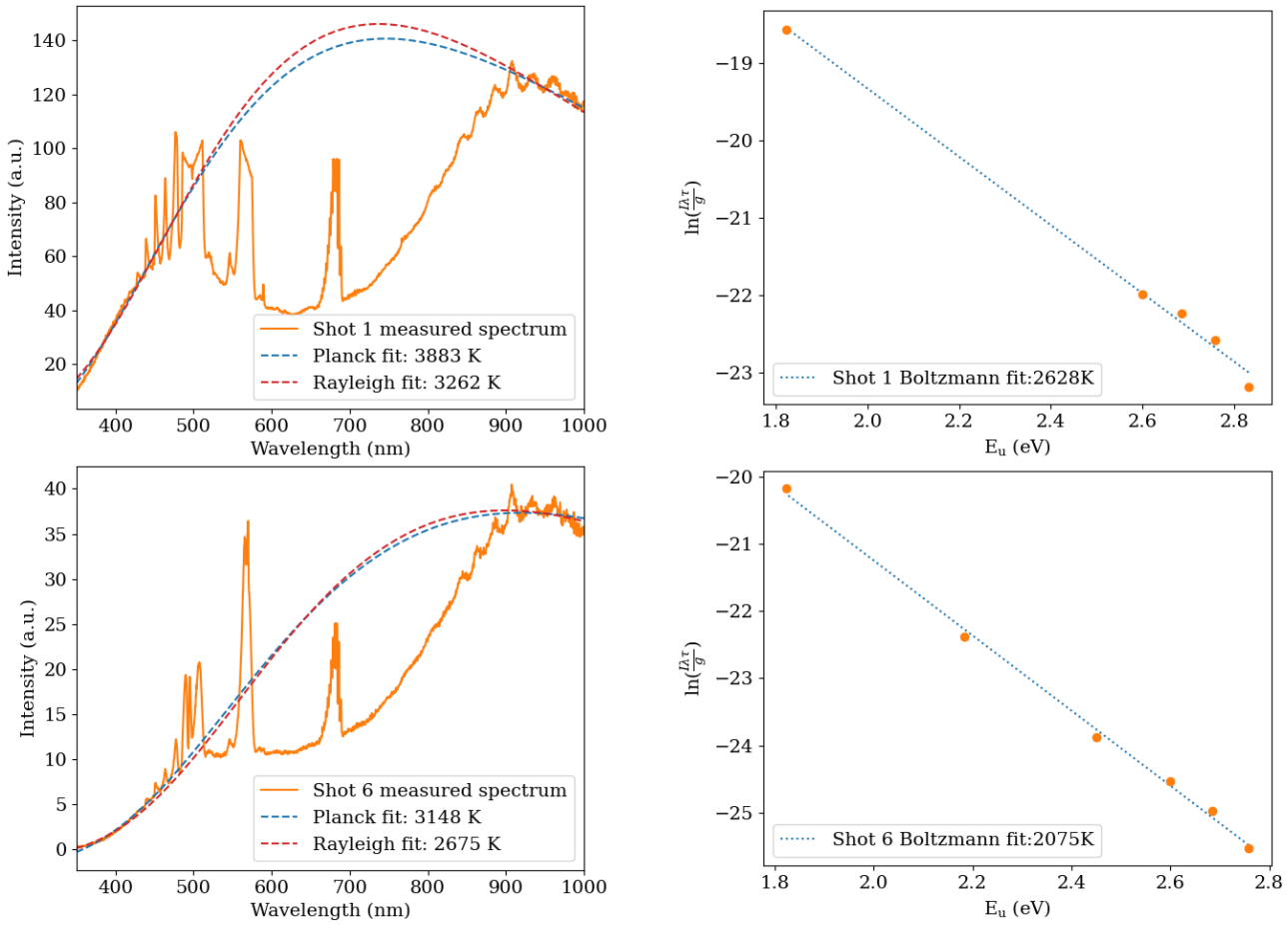


*Figure 4. Example spectra, gray-body fits, and Boltzmann plots for first and last shots.*

for the influence of particle size on the emissivity in the limiting cases, it doesn't fully account for other processes that may affect $\epsilon(\lambda)$. Furthermore, the spectral fits assume a constant, wavelength independent $\epsilon$, while the spectral calibration did not account for the attenuation caused by soot buildup on the window. To account for these potential sources of error, the relative emissivities of the two spectral bands used for fitting were allowed to vary by up to 50% (i.e. $2/3 \geq \epsilon_{IR}/\epsilon_{UV} \leq 3/2$). Repeating the fitting procedure using these corrected $\epsilon$ values results in an estimated temperature uncertainty interval spanning almost $\pm 20\%$ if the extreme values of $T_P$ and $T_R$ are taken as upper and lower bounds.

The Boltzmann plot evaluation is in general less sensitive to most sources of error, due to the logarithmic dependence of the temperature on measured intensity $I$. Most band intensities were measured with high signal-to-noise, and covered a reasonably large upper state energy range ($\Delta E_u \approx 1\,\text{eV}$), which limited uncertainty coming from the measurement and fitting procedure to $\sim \pm 100\,\text{K}$. It has been shown that one of the largest sources of error is often in the basic molecular data itself, (i.e. the values of $\tau_u$ reported in Table 1), which can have uncertainties of up to 30%, however this corresponds to only 3% or less uncertainty in temperature [16]. Accounting for the potential influence of other aforementioned sources of error, the uncertainty in the values of $T_B$ can be conservatively estimated at $\sim 10\%$

### 3.3. Discussion

Accounting for these mutual uncertainties does not fully explain the systematic disagreement observed between $T_P/T_R$ and $T_B$, so alternative explanations should be considered. One possibility is that the two evaluation methods probe the temperatures of different particles in the exhaust gas, which are not necessarily the same. The continuum emission is believed to originate primarily from relatively large $(10-100\,\text{nm})$ soot particles, an understanding that is consistent with both the present optical measurements and with morphological soot properties noted in other studies [7]. Conversely, the band emission used in the Boltzmann plot evaluation originates from excited gas-phase CuF molecules, presumably in thermal equilibrium with the exhaust gas. The initial energy distribution of the soot particles may already differ from that of the exhaust gas, as it can be influenced by the formation process. As the exhaust mixture propagates from the heating volume to the measurement region, its temperature drops as it undergoes collisions with the cooler

fill gas [2]. The larger soot particles can be expected to have much longer thermal relaxation times in comparison to the gas itself, potentially giving rise to a two-temperature distribution of warm soot particles surrounded by a cooler gas flow that produces the observed temperature mismatch. Regardless of the cause of this temperature discrepancy, the values of $T_B$ can be assumed to have higher accuracy than the values of $T_P$ or $T_R$, and to provide the most reliable measure of the gas temperature, which is of the most consequence for dielectric recovery conditions in CB exhaust volumes.

## 4. Conclusions

In this work, optical emission spectroscopy measurements of exhaust gas temperatures were performed immediately after high current interruption in a model circuit breaker filled with $CO_2/O_2$. Two evaluation methods were presented: one based the relative intensity of continuum emission in the ultraviolet and infrared, and another using the intensity ratio of emission bands produced by CuF molecules formed in the exhaust gas. The two methods yielded temperatures ranging from 3000 K to 4000 K and 2000 K to 2600 K, respectively. This temperature disagreement lies outside of the estimated mutual uncertainty interval, which may be explained by a two-temperature distribution with warmer soot particles suspended in a cooler gas flow. Both evaluation methods indicate a direct correlation between the pressure buildup generated inside the heating volume and the exhaust gas temperature. Future investigations will aim to more conclusively establish the nature and accuracy of the measured temperatures, and extend the study to look at the spatial distribution and time-evolution using additional diagnostics, including pyrometry and high-speed imaging techniques.

### Acknowledgements

The authors would like to thank Torsten Votteler, Martin Seeger, Mahir Muratovic, Oliver Weber and Marcelo Buffoni for their valuable contributions to this work.

### References

[1] M. Seeger, R. Smeets, J. Yan, et al. Recent Trends in Development of High Voltage Circuit Breakers with $SF_6$ Alternative Gases. *Plasma Physics and Technology Journal*, 4:8–12, 01 2017. doi:10.14311/ppt.2017.1.8.

[2] K. Soni, M. Seeger, and M. Schwinne. Study of exhaust gas temperature in a prototype $CO_2$/C4-FN/$O_2$ circuit breaker using pyrometry. *IET Conference Proceedings*, 2023, 12 2023. doi:10.1049/icp.2024.0480.

[3] M. Seeger, T. Votteler, S. Pancheshnyi, et al. Breakdown in $CO_2/O_2$ and $CO_2/O_2/C_2F_4$ mixtures at elevated temperatures in the range 1000–4000K. *Plasma Physics and Technology*, 6:39–42, 07 2019. doi:10.14311/ppt.2019.1.39.

[4] Y. Hayashi, M. Watanabe, A. Okino, and E. Hotta. Dynamics of exhaust gas generated by arc extinction. *Journal of Applied Physics*, 90(10):4966–4972, 11 2001. doi:10.1063/1.1412276.

[5] Y. Tanaka, R. D. Smirnov, A. Y. Pigarov, and M. Rosenberg. Influence of emissivity on behavior of metallic dust particles in plasmas. *Physics of Plasmas*, 15(7):073704, 07 2008. doi:10.1063/1.2946435.

[6] F. Goulay, P. Schrader, and H. Michelsen. Effect of wavelength dependent emissivity on inferred soot temperatures measured by spectrally resolved laser induced incandescence. *Applied Physics B: Lasers and Optics*, 100:655–663, 09 2010. doi:10.1007/s00340-010-4119-2.

[7] S. Chippett and W. Gray. The size and optical properties of soot particles. *Combustion and Flame*, 31:149–159, 1978. doi:10.1016/0010-2180(78)90125-6.

[8] R. E. Steele and H. P. Broida. Chemiluminescence and photoluminescence of CuF. *The Journal of Chemical Physics*, 69(6):2300–2305, 09 1978. doi:10.1063/1.436939.

[9] F. Ahmed, R. F. Barrow, A. H. Chojnicki, et al. Electronic states of the CuF molecule. I. analysis of rotational structure. *Journal of Physics B: Atomic and Molecular Physics*, 15(21):3801, nov 1982. doi:10.1088/0022-3700/15/21/006.

[10] C. Dufour, J. Schamps, and R. F. Barrow. Electronic states of the CuF molecule. II. nature of the observed states. *Journal of Physics B: Atomic and Molecular Physics*, 15(21):3819, nov 1982. doi:10.1088/0022-3700/15/21/007.

[11] J. Delaval and J. Schamps. Ab initio computation of radiative lifetimes of the valence electronic states of CuF. *Chemical Physics*, 100(1):21–32, 1985. doi:10.1016/0301-0104(85)87020-8.

[12] J. Schamps, J. Delaval, and O. Faucher. A calculation of radiative lifetimes of electronically excited rovibronic levels of CuF. *Chemical Physics*, 145(1):101–110, 1990. doi:10.1016/0301-0104(90)80121-D.

[13] D. S. Talaga and J. I. Zink. Copper fluoride luminescence during UV photofragmentation of $Cu(hfac)_2$ in the gas phase. *Inorganic chemistry*, 35 17:5050–5054, 1996. doi:10.1021/ic9515362.

[14] R. Methling, N. Götte, and D. Uhrlandt. Ablation-dominated arcs in $CO_2$ atmosphere—part II: Molecule emission and absorption. *Energies*, 13(18), 2020. doi:10.3390/en13184720.

[15] J. T. Engelbrecht, D. Kumari, and C. M. Franck. Optical characterization of actively cooled switching arcs in $SF_6$ alternatives. *Journal of Physics D: Applied Physics*, 58(10):105210, jan 2025. doi:10.1088/1361-6463/ada450.

[16] J. T. Engelbrecht, S. Gortschakow, R. Methling, et al. Study of transient arc properties near current zero in an experimental $CO_2$ high-voltage circuit breaker. *Journal of Physics D: Applied Physics*, 58(15):155207, mar 2025. doi:10.1088/1361-6463/adbb00.